

# Quantifying the benefits of Wind Power diversity in New Zealand

Dougal McQueen and Alan Wood

Electric Power Engineering Centre, University of Canterbury, NEW ZEALAND.

Email: dougal.mcqueen@hylandmcqueen.co.nz

**Abstract**—A common conclusion from wind integration studies is the benefit of spatial diversification of Wind Power Plants for power systems. However, few of these studies quantify the benefit that may be apparent from different wind power portfolios. To quantify that benefit, temporally and spatially accurate models of wind power are required. A wind power model is constructed starting with wind speed time-series extracted from the ECMWF-interim reanalysis model. The wind speed time-series are interpolated, scaled, and imputed such that they are representative of the wind incident on the Wind Power Plants. Imputation is performed using a Wavelet Multi-Resolution Analysis approach that ensures temporally consistent correlations while accommodating heteroskedasticity. The wind speed time-series are transformed to power by applying wind power plant power curves, low pass filters, and a Markov Chain model for operational efficiency. Simulated wind power time-series are validated using a set of measurements made at Wind Power Plants in New Zealand. The wind power model is used to simulate power time-series for 2 GW portfolios of wind power plants representing compact, disperse, diverse, and Business As Usual portfolios. Metrics for dependability, variability, and predictability are used to quantify the benefits of spatial diversification.

## I. INTRODUCTION

Wind power is one of the least cost methods for electricity generation and along with its scalability and lack of emissions this has led to large numbers of Wind Power Plants (WPP) being integrated into power systems. However, the intermittency of wind and the largely passive reaction of Wind Turbines (WT) leads to certain levels of variability and unpredictability in wind power output. Hence wind power can require additional reserves and interruptible loads, referred to as secondary control mechanisms [1], so that power quality is well managed. As power plants capable of supplying reserves can have large capital costs, and lead times for building plant are large, it is requisite that integration studies are undertaken to quantify the necessary reserves for envisaged wind power development scenarios. Integration studies that focus on reserves requirements are classified as Unit Commitment and Economic Dispatch studies [2].

The Wind Generation Investigation Project (WGIP) was undertaken in New Zealand (NZ) by the system operator to address concerns over large ramp rates observed in the Manawatu during 2004 [3], [4]. The WGIP, conducted in 2007, was accompanied by other integration studies by various stake holders [5] [6] [7]. The number of integration studies conducted worldwide lead to the IEA producing guidelines to assist system operators with managing wind power integration [2]. Many integration studies conclude that one way of reducing stress on the power system is through spatial diversification [8] [9]. However, most studies fall short of quantifying that benefit.

Secondary control of the NZ power system is primarily achieved by the New Zealand Electricity Market (NZEM). The NZEM uses 30 minute windows, each window constituting a trading period, with gate closure 2 hours prior to the trading period. As changes in demand and generation are faster than the reaction of the NZEM, a reserves market with a window of 5 minutes is also operated. These temporal spans provide the basis for metrics of variability (changes in power output or ramps over 5 minutes), and predictability (the error in power forecasts with a 2 hour horizon using a 30 minute window). For this study power forecasts are made assuming persistence, as even the most advanced forecasting methods provide little additional benefit for horizons of less than 6 hours [10]. A dependability metric is also used; describing how much power can be relied upon at any time and is measured using the standard deviation of power.

To quantify the benefits of spatial diversification sets of wind power time-series are required. The sets of time-series must replicate the variability of the Wind Power Plants (WPP), the spatio-temporal correlations between WPPs, and be congruent with other forms of generation and demand so that the impact on the power system can be evaluated.

## II. SCENARIOS

To demonstrate the potential benefits from spatial diversification, of WPPs in New Zealand, scenarios for wind power development have been constructed. The location of the WPPs in the scenarios are taken from media releases that cover either commissioning, consenting, or proposal. Four scenarios have been developed, each comprising 2 GW capacity. A compact scenario comprises 7 WPPs, nominally 300 MW, located in the lower North Island, a disperse scenario comprises 7 WPPs spread throughout NZ, and a diverse scenario comprises 70 WPPs (nominally 30 MW) spread throughout NZ. A Business As Usual scenario comprises the set of WPPs presently operational, plus WPPs with capacities consistent with those operational, to make up the 2 GW portfolio. The scenarios are presented in Figure 1. It is assumed that the WPPs comprise approximate square arrays of Vestas V80 2.0 MW wind turbines [11], with capacity factors of 40 %.

## III. WIND SPEED SIMULATION

Coherent sets of wind power time-series are obtained by simulating wind speed time-series for each WPP and transforming these to power. The wind speed time-series must be representative of the wind incident on the WPPs individually and have correlations that are temporally and spatially consistent. Coarse resolution wind speed time-series

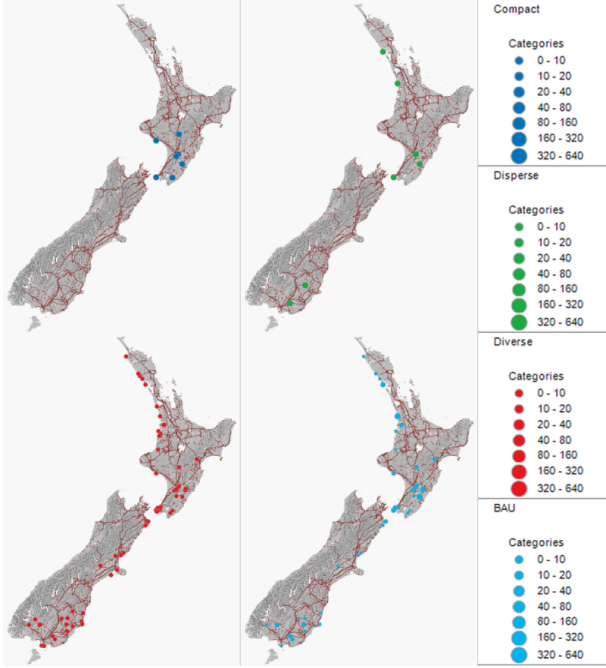


Fig. 1. Scenarios each comprising 2 GW capacities. Top left: compact, top right: disperse, bottom left: diverse, bottom right: business as usual (BAU).

are extracted from the ECMWF ERA-interim Numerical Weather Prediction (NWP) model, which is freely available and provides wind speeds representative of a 10 m height, on a grid with reasonable spatial (0.7x0.7 degree) and temporal resolutions (6 hour) [12]. The wind speed time series (WSTS) require interpolation to WPP locations, scaling to be representative of the wind incident on the WPP, and imputation to obtain the desired temporal resolution. Many integration studies increase temporal and spatial resolutions using meso-scale models [8], however here numerical methods are used that require fewer resources.

The WSTS are interpolated using two dimensional cubic splines, and scaled by a ratio so that the resultant power time-series have capacity factors equal to 40 %. The scaling of a wind speed time-series is shown in Equation 1. A set of wind speed measurements made at 21 meteorological masts, located throughout New Zealand and erected for wind prospecting purposes, are used to validate the interpolation function as detailed by McQueen [13]. The dataset is similar to that used in the Wind Generation Integration Project [3].

$$u_N(t) = S_{(\theta, N)} \cdot u_M(t) \quad (1)$$

Where  $u$  is the wind speed,  $N$  is the turbine index,  $t$  is time,  $\theta$  is the wind direction sector,  $S$  is the speed up, and  $M$  denotes the meteorological mast.

The imputation of the WSTS increases the temporal resolution from 6 h to 5 min. A model that is spatially and temporally congruent is developed which in effect characterises turbulence. The model applies Wavelet Multi-resolution Analysis (WMA) and is validated using the set of wind speed measurements [13].

A wavelet is a finitely bounded function that is square integrable as presented in Equation 2. This mean that the

wavelet is a short sequence with an oscillatory shape, with some wavelets being similar to a discretised damped sine wave. A wavelet transform decomposes a time-series, by deconvolving the time-series by the wavelet, resulting in a residual time-series and a wavelet series. The residual time-series and wavelet series have temporal resolutions half that of the starting time-series. Wavelets are numerically particular so that the space defined by the scale and translation the wavelet series is orthogonal to the residual time-series. The scale can be considered the wavelet space equivalent of frequency, and the translation the wavelet space equivalent of time.

$$\{\psi_{j, \tau}(t) = \frac{1}{\sqrt{2^j}} \psi\left(\frac{t - 2^j \tau}{2^j}\right)\}_{(j, \tau) \in \mathbb{Z}^2} \quad (2)$$

Where  $\psi$  is the mother wavelet,  $j$  is the scale,  $\tau$  is the translation, and  $\mathbb{Z}$  is the set of integers.

$$\langle u(\tau, 2^j), \Psi(j, \tau) \rangle = \int_{-\infty}^{\infty} u(t) \frac{1}{\sqrt{2^j}} \psi^* \left( \frac{t - \tau}{2^j} \right) dt \quad (3)$$

Where  $\Psi$  is the wavelet coefficient series,  $t$  is time, and  $*$  denotes the complex conjugate.

The wavelet transform is applied recursively to a wind speed time-series, by dilating the wavelet, so that a set of wavelet series and a residual time-series, with a coarse temporal resolution, is obtained. The set of wavelet series has scales that are spread dyadically, i.e. having central scales that are spread as powers of two as expressed in Equation 3. Here, the wavelet decomposition is structured so that the temporal resolution of the residual time-series is 6 h to marry with the ECMWF-interim model resolution. Hence, the wavelet series have scales of 6, 3, 1.5, 0.75, and 0.375 hours.

The wavelet decomposition of the total wind speed data set results in a data structure with three dimensions: scale, translation, and the distance between time-series. This structure is identified using measures of cross-correlation (expressed in Equation 4), auto-correlation (see Equation 5), and correlation (as expressed in Equation 6); respective of scale, translation, distance. Simulation of a three dimensional data-structure is complicated, however the dimensionality of the data set is effectively reduced by minimising the cross-correlation by careful selection of the wavelet. Of all the wavelets in the Wavelet toolbox for Matlab [14] the Beylkin wavelet results in the lowest cross-correlation, sufficiently small to allow wavelet series of adjacent scales to be considered independent.

$$R(\Psi_n(j), \Psi_n(j+1)) = \sum_{\delta = [-\frac{1}{4}, \frac{1}{4}]} \sum_{\tau=1}^T \{(\Psi_n(j, \tau) - \overline{\Psi_n(j, \tau)}) (\Psi_n(j+1, \tau + \delta) - \overline{\Psi_n(j+1, \tau + \delta)})\} \quad (4)$$

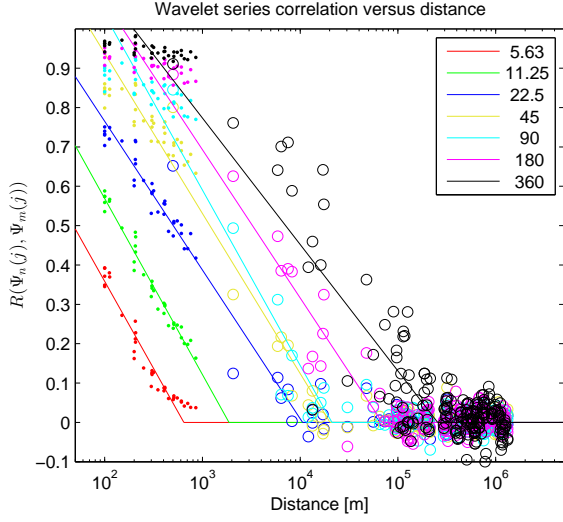


Fig. 2. Correlation as a function of separation distance for wavelet series with scales from 5.63 min through 360 min. Points represented using circles derive from the wind speed data set, points represented using dots derive from the Mt Stuart data. Lines present best fit log-linear regressions.

$$R(\Psi_n(j, \tau), \Psi_n(j, \tau + \delta)) = \sum_{\tau=1}^T \{(\Psi_n(j, \tau) - \overline{\Psi_n(j, \tau)}) (\Psi_n(j, \tau + \delta) - \overline{\Psi_n(j, \tau + \delta)})\} \quad (5)$$

Where  $R$  is the Pearson's correlation coefficient,  $n$  is a measurement, and  $\Psi_n(j, \tau)$  is the temporal average of the wavelet coefficients.

$$R(\Psi_n(j), \Psi_m(j)) = \sum_{\tau=1}^T \{(\Psi_n(j, \tau) - \overline{\Psi_n(j, \tau)}) (\Psi_m(j, \tau) - \overline{\Psi_m(j, \tau)})\} \quad (6)$$

Where  $m$  is a second measurement.

Using the decomposition of the measured wind speed time-series, it is found that the relationship between the mean square, or power, of the wavelet series and the scale is well approximated by a log-log linear function, similar to Kolmogorov's law [15]. The assumption of a log-log linear function allows the WMA model to be extrapolated [13]. The WMA model is extrapolated to scales of 11.25 min and 5.26 min, so that the simulated time-series have a temporal resolution of 1.81 min; greater than the 5 min criteria for determining ramp rates. And, it is found that the correlation at any scale is well approximated by a log-linear function of the separation distance between wind speed measurement locations, as shown in Figure 2. As the minimum separation distances in the WGIP dataset are greater than 1 km and the dataset does not resolve scales of 11.25 and 5.26 min, additional data from the Mt Stuart wind farm is used to inform the log-linear correlation functions [13]. The distance relationship is a wavelet domain equivalent to Davenport's model of coherence.

The decomposition of the time-series into a set of wavelet series, allows a relationship between the wavelet series and

the residual time-series to be established. It is found that the magnitude of the wavelet series is related to the magnitude of the residual time-series, and this is modelled using a Taylor's transform as shown in Equation 7. The application of the Taylor's transform accounts for gustiness, which is literally interpreted in the statement "it is gusty when it is windy". If the Taylor's transform is not applied then the simulated wind speed time-series will be homoskedastic, and the resulting power time-series will not have temporally correct ramp rates.

$$\Psi_n^{(T)}(j, \tau) = \frac{\Psi(j, \tau)}{\bar{u}(t)^a} \quad (7)$$

Where  $a$  is the Taylor exponent, and  $T$  represents the Taylor transformed variable.

$$\Psi_n^{(TJ)}(j, \tau) = \gamma + \eta \sinh^{-1}\left(\frac{\Psi_n^{(T)}(j, \tau) - \epsilon}{\lambda}\right) \quad (8)$$

Where  $J$  represents the Johnson transformed variable,  $\gamma$  and  $\eta$  are shape parameters,  $\epsilon$  is the location parameter, and  $\lambda$  is the scale parameter.

Sets of the wind speed time-series are simulated by constructing a wavelet structure for each WPP. The residual time-series in the wavelet structure is filled using values from the interpolated and scaled ECMWF-interim wind speed time-series. Each wavelet series in the wavelet structure is filled with a sequence of random numbers that have auto-correlations and correlations enforced using a Correlated Innovation Matrix (CIM) method as shown in Equation 9. The Box-Jenkins method using correlograms and partial-correlograms identifies the  $\Psi_n^{(TJ)}(j)$  series as an over-differenced AR processes with a model order of 1 [16]. The CIM method works by multiplying the innovation matrix in the AR process by the Cholesky decomposition of the correlation matrix calculated using the log-linear distance relationship.

$$\begin{aligned} \Psi_n^{(TJ)}(j, \tau) = & A_\alpha(j) \cdot \Psi_n^{(TJ)}(j, \tau - \alpha) + \\ & A_{\alpha-1}(j) \cdot \Psi_n^{(TJ)}(j, \tau - (\alpha - 1)) + \dots + \\ & A_1(j) \cdot \Psi_n^{(TJ)}(j, \tau - 1) + \zeta \cdot e_t \end{aligned} \quad (9)$$

Where  $A_\alpha$  is the AR coefficient of order  $\alpha$ ,  $\zeta$  is the CIM weighting matrix, and  $e$  is the innovation matrix.

The shape of the probability distributions for the measured wavelet series are non-Gaussian. And, as simulations are initiated from normally distributed random numbers, a Johnson transform, as shown in Equation 8, is applied to modify the simulated wavelet-series so that the shape of their probability distributions approximates that of the measured [13]. Inverse wavelet transformations are then applied to obtain a wind speed time-series for each WPP.

#### IV. WIND SPEED TO POWER TRANSFORM

Wind speed time-series are transformed to power by characterising steady state and dynamic characteristics of the WPP separately. The steady state transform, which accounts

for topography, is modelled using a generic WPP power curve. The generic WPP power curve is obtained by applying a Gaussian distribution of speed-ups to the wind turbine power curve as shown in Equation 10. A speed-up standard deviation of 0.065 is obtained from measurements made at the Mt Stuart Wind Farm and the mean speed-up equals one.

$$P_S(u) = \int_{q=0}^1 P(u \cdot S_{\mu_g, \sigma_g}(q)) dq \quad (10)$$

Where  $P$  is power,  $S$  is a speed-up,  $d$  is wind direction sector, and  $q$  is probability.

The dynamic transform characterises the inertial and spatial integration of the WPP, and is modelled using a simple Low Pass Filter (LPF) as shown in Equation 11. The LPF multiplier ( $M_c$ ) and exponent ( $M_e$ ) are calculated by simulating power time-series for WPPs comprising square arrays of Vestas V80 2.0 MW turbines. The WMA model is used to simulate the WSTS incident on each WT. These WSTS are converted to power using the WT power curve and aggregated to find a WPP power time-series. A power time-series is simultaneously derived using a WPP power curve applied to a single turbine WSTS that has been low pass filtered. The LPF multiplier and exponents are found by minimising difference in the Power Spectral Densities (PSD) between the two power time-series, with resulting LPF multiplier of 151 s and exponent of 0.57 [13].

$$w_{\omega'} = F' \left\{ F(u) \frac{1}{1 + M_c \cdot N^{M_e} \cdot \omega} \right\} \quad (11)$$

Where  $\omega$  is frequency,  $F$  denotes a Fourier transform,  $F'$  the inverse Fourier transform,  $N$  the number of turbines,  $M_c$  the time constant, and  $M_e$  the low pass filter exponent.

The simulated power from the WPP ( $P$ ) is the sum of the power supplied by all of the wind turbines given unrestricted operation. In reality a WPP incurs losses due to electrical efficiency, and WPP operation. Electrical losses are relatively small and vary with the power, and are accounted for in WPP power curve. The operational losses occur due to faults and maintenance of the WPP, and can result in large instantaneous changes in output. A Markov Chain (MC) model for the operational efficiency is constructed using measurements made at a set of eight WPPs, similar to the model described by Sulaeman [17]. Time-series of the operational efficiency are obtained for each WPP and percentile values calculated. Transition matrices are formed from these and the average of the transition matrices used to define a generic MC model. The mean operational efficiency from measurements is 95 % and this is replicated by the MC model [13].

## V. VALIDATION

Measured power time-series, from a set of eight WPPs in New Zealand, are used to validate the wind power model. The measurements have a temporal resolution of 5 min and a duration of 7 months. Power time-series are simulated for the period that is coincident with the measured power time-series. In summary, WSTS are derived from the ECMWF-interim NWP model, interpolated, scaled and imputed. The

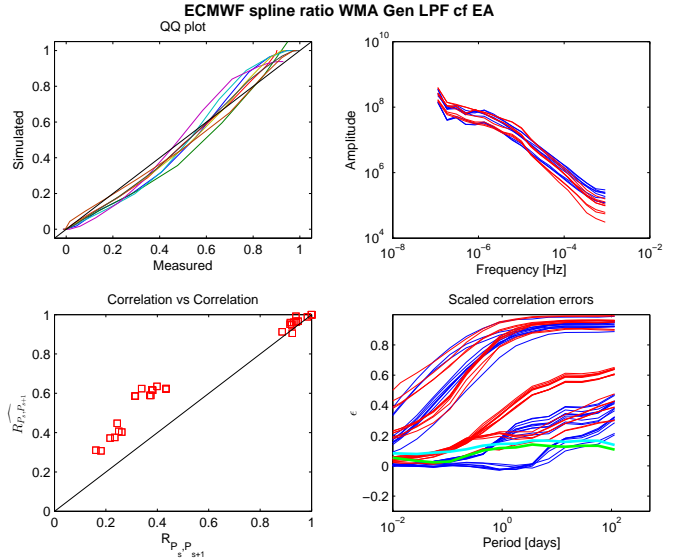


Fig. 3. Wind power validation

WSTS are smoothed using a LPF, transformed to power using generic WPP power curves, and modified to account for the operation efficiency using the MC model. The WSTS are scaled such that the total energy of a simulated time-series equals that of the equivalent measured.

The wind power time-series are compared with the measured time-series in Figure 3. The top left graph presents a Quantile-Quantile (QQ) plot, each line representing a WPP, which shows good agreement between the probability distribution functions of the simulated and measured time-series. The top right graph presents a periodogram with PSDs derived from measured values shown as blue lines, and from simulations as red lines. The simulated PSDs tend to underestimate variability for frequencies above  $10^{-4}$  Hz, reflecting the assumption that WPPs comprise square arrays which results in WPPs with less spatial extents than their real world counterparts. The bottom left graph presents simulated versus measured correlations as shown in Equation 12. It is seen that the model generally over predicts the correlation between power time-series, i.e. real world WPPs behave with greater independence than the simulations suggest.

$$R_{P_r, P_s} = \frac{\sigma_{P_r, P_s}}{\sigma_{P_r} \cdot \sigma_{P_s}} \quad (12)$$

Where  $R$  is the Pearson's correlation coefficient,  $r$  and  $s$  are different WPPs,  $\sigma_{P_r}$  is the variance of power from WPP  $r$ , and  $\sigma_{P_r, P_s}$  is the covariance between the time series.

A measure of the correlation as a function of the temporal span is the Scaled Correlation. For a particular scale power time-series pairs are broken into segments of the corresponding length (as presented in Equation 13), the correlation coefficient for each pair of segments is derived, and the average of these correlation coefficients calculated as presented in Equation 14. The lower right graph presents scaled correlations. The blue lines represent the scaled correlations between pairs of power time-series from measurements and the red lines result from simulations. The scaled correlations show that at low scales the correlation between WPPs

is small and increases as the scale becomes larger. An indication of the difference between the sets of simulated and measured scaled correlations is given by the mean bias (shown by the green line), and the Root Mean Squared (shown using the cyan line). For scaled correlations with periods of less than 6 h simulated data derive from the WMA model and those with periods longer than 6 h derive from the NWP model. This shows the WMA model accurately models the scaled correlations while there are greater errors introduced from the NWP model.

$$K(j) = \text{floor}\left(\frac{T}{j}\right) \quad (13)$$

Where  $K$  are the power time-series segment,  $T$  is the total time, and  $j$  is the scale.

$$R_{P_r, P_s}^-(j) = \frac{1}{K} \sum_{k=1}^K R_{P_r(k), P_s(k)} \quad (14)$$

Where  $R_{P_r, P_s}^-(j)$  is the scaled correlation between power time-series from WPPs  $r$  and  $s$  at a scale of  $j$ .

## VI. RESULTS

The wind power model is used to simulate power time-series for each of the envisaged WPPs in the scenarios for the year of 1998. The results presented in Figure 4, where the top left graph presents a short extract during which Cyclone Bola crossed New Zealand. This storm caused significant damage and it is of interest to see how it might have impacted the power the various scenarios. It is seen that the power from a compact scenario has a much greater changes in power than the disperse or BAU scenarios. The diverse scenario provides the smoothest power output. The top right graph presents probability density functions for the power over the entire year of 1998. It is seen that a compact scenario has a more extreme shape to its probability distribution, with greater chance of near zero and near maximum outputs than the other scenarios. The differences in the shapes of the PDFs is reflected in the standard deviation for the scenarios presented in Table I where it is seen that a compact scenario has a standard deviation 28 % greater than the diverse scenario. This means that a compact scenario of WPPs will produce power with lower dependability than a disperse or diverse scenarios.

The lower left graph presents ramp rates and it is seen that the compact and disperse scenarios have near identical variability, whereas the diverse scenario results in ramp rates 25% of the compact scenario. The distribution of ramp rates has a slight positive bias; the magnitude of ramp rate increases with a probability of occurrence equating to once per week is 10% greater (for the disperse and BAU scenarios) than the equivalent ramp down.

The lower right graph presents forecast errors for the scenarios; the forecast errors for the compact scenario are 45% greater than for the other scenarios. It is seen that the distribution of forecast errors is skewed in favour of negative errors, the once per week forecast errors having approximately 20% greater magnitude of under-prediction than the equivalent over prediction.

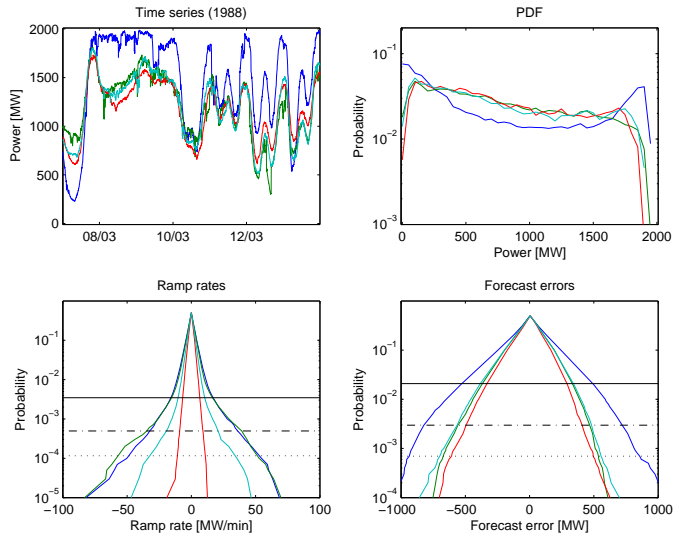


Fig. 4. Power simulation results for scenarios: blue (compact), green (disperse), red (diverse), cyan (BAU). Horizontal solid black lines correspond to events with a probability of occurrence of once per day, dash-dotted with events that occur once per week, and dotted with events that occur once per month.

The BAU case exhibits a balance between the diverse and compact scenarios with a variance 83% of the compact scenario but 6% higher than the diverse scenario, ramp rates are half those for the compact scenario but twice the diverse scenario, and forecast errors are 75% of the compact scenario and 15% greater than the diverse scenario.

Scenario	Compact	Disperse	Diverse	BAU
Mean [MW]	799	799	799	799
Standard deviation [MW]	664	534	519	551
+ve ramp rate [MW]	-33	-32	-8	-18
-ve ramp rate [MW]	35	37	8	20
+ve forecast error [MW]	-758	-514	-487	-563
-ve forecast error [MW]	636	438	397	457

TABLE I  
RESULTS FROM WIND POWER SIMULATIONS FOR SCENARIOS. RAMP RATES AND FORECAST ERRORS ARE REPRESENTATIVE OF EVENTS WITH A PROBABILITY OF OCCURRENCE OF ONCE PER WEEK.

## VII. CONCLUSION

The integration of Wind Power Plants into electricity networks can lead to the need for increased reserves so that power quality is managed. Many integration studies conclude that the impact of wind power on the power system can be reduced through spatial diversification. However, few of these studies provide methods for comprehensively quantifying the impact of specific wind power portfolios.

This paper has outlined a method that simulates power time-series with the correct spatial and temporal correlations. The method uses Wind Speed Time-Series from the ECMWF-interim Numerical Weather Prediction model. The WSTS are interpolated, scaled, and imputed so that they are representative of the wind speed incident on WPPs. The imputation uses a Wavelet-Multi-resolution Analysis approach ensuring temporally and spatially consistent correlation. The WSTS are transformed to power using a Low Pass Filter applied to the WSTS, a generic WPP power curve, and a Markov Chain model to capture operational efficiency.

Power time-series are simulated and compared with a set of measured power time-series from Wind Power Plants located in New Zealand, showing the model has good accuracy. The model is applied to simulate 2 GW portfolios of wind power scenarios in New Zealand. It is shown that a compact portfolio will result in lower dependability, a disperse portfolio will have greater predictability, and a diverse portfolio will have lower variability. The Business-As-Usual scenario indicates the development of wind power in New Zealand to date has achieved some of the benefits of spatial diversification, however greater benefits could be accrued through coordinated development.

#### ACKNOWLEDGMENT

This work is part of the GREEN Grid project funded by Ministry Business Innovation and Employment, New Zealand. [www.epecentre.ac.nz/greengrid](http://www.epecentre.ac.nz/greengrid)

#### REFERENCES

- [1] T. Ackermann, *Wind Power in Power Systems*. Wiley, 2005.
- [2] H. Holttinen, "Expert group report on recommended practices; 16. wind integration studies," 2013, [https://www.ieawind.org/task\\_25.html](https://www.ieawind.org/task_25.html).
- [3] D. McQueen, P. Wong Too, and G. White, "Wind power variability and forecast accuracy in new zealand," 2007, <http://www.ea.govt.nz/our-work/programmes/pso-cq/wgip/>.
- [4] Transpower, "Effect of unpredictability of wind generation output on pre-dispatch processes, investigation 1- part a," 17 November 2015 2007.
- [5] I. M. Rasmussen and M. H. Windolf, "Wind power integration in new zealand : a scenario analysis of 15-25 % wind power in the electricity market in 2025," Masters, Technical University of Denmark, 2008.
- [6] G. Strbac, D. Pudjianto, A. Shakoob, M. Castro, and G. Waipara, "The system impacts and costs of integrating wind power in new zealand," 2008, <http://www.epoc.org.nz/workshops/ww2008/NZWindIntegrationCostsPhase-IIReportFinal.pdf>.
- [7] E. Link and M. NZ, "Wind energy integration in new zealand," 2005, <http://citeseerx.ist.psu.edu/viewdoc/download?doi=10.1.1.132.9261\&rep=rep1\&type=pdf>.
- [8] J. Dowds, P. Hines, T. Ryan, W. Buchanan, E. Kirby, J. Apt, and P. Jaramillo, "A review of large-scale wind integration studies," *Renewable and Sustainable Energy Reviews*, vol. 49, pp. 768–94, 2015.
- [9] J. Manobianco, C. Alonge, and J. Frank, "Development of regional wind resource and wind plant output datasets for the hawaiian islands," 2010, [http://www.nrel.gov/electricity/transmission/oahu\\_wind.html](http://www.nrel.gov/electricity/transmission/oahu_wind.html).
- [10] Metservice, "Response to consultation paper: Wind forecasting and integration options," 2010, <https://www.ea.govt.nz/dmsdocument/6029>.
- [11] Vestas, "General specification,v80-2.0 mw 50 hz vcs," 2010.
- [12] D. Dee, "The era-interim reanalysis: configuration and performance of the data assimilation system," *Quarterly Journal of the Royal Meteorological Society*, vol. 137, no. 656, pp. 553–97, 2011.
- [13] D. McQueen, "Quantifying the benefits from the spatial diversification of wind power in new zealand," Ph.D. dissertation, Dept. Elec. and Comp. Eng., University of Canterbury, 2017.
- [14] S. Mallat, *A Wavelet Tour of Signal Processing, Third Edition: The Sparse Way*. Academic Press, 2008.
- [15] R. B. Stull, *An introduction to boundary layer meteorology*, ser. Atmospheric sciences library. Kluwer Academic, 2003.
- [16] H. Ltkepohl, *New Introduction to Multiple Time Series Analysis*. Springer, 2007.
- [17] S. Sulaeman, M. Benidris, and J. Mitra, "A method to model the output power of wind farms in composite system reliability assessment," in *North American Power Symposium (NAPS), 2014*, 2014.